

Release of potential shearing instability in warm frontal zones

By D. CHAPMAN and K. A. BROWNING*

University of Reading, UK

(Received 16 February 1998; revised 17 November 1998)

SUMMARY

Potential shearing instability (PSHI) exists in the atmosphere when the Richardson number in a stably stratified shear layer would be less than $\frac{1}{4}$ if the layer were lifted to saturation. Sometimes the air entering a warm frontal zone near the position of the surface warm front is initially unsaturated, its Richardson number is greater than $\frac{1}{4}$, but PSHI exists over a deep layer. This paper presents a study of a warm frontal zone using observations from the high-resolution Doppler radar at Chilbolton, supported by radiosondes and output from the mesoscale version of the operational United Kingdom Meteorological Office Unified Model. Very large-amplitude Kelvin–Helmholtz billows were observed to form where the PSHI was realised following the onset of saturation. The billows were probably intense enough to be a hazard for air traffic and an important source of momentum transfer. Rough estimates from the radar of vertical momentum fluxes due to the billows are shown to be broadly consistent with measurements by the same radar of the change in velocity profile across the frontal zone from start to end of the billow train. The present version of the Unified Model does not parametrize vertical mixing due to shearing instability in the free atmosphere; this may be an important omission.

KEYWORDS: Doppler radar Kelvin–Helmholtz billows Mesoscale model Mixing Shearing instability Warm front

1. INTRODUCTION

Over the last 30 years, the existence of billows in the atmosphere has been demonstrated from aircraft measurements (Browning *et al.* 1973a; Hardy *et al.* 1973; Nielsen 1992) and radar (Atlas *et al.* 1970; Browning 1971; James and Browning 1981), and by visual observation of associated clouds (e.g. Ludlam 1967, 1980). The existence of large-amplitude billows in the atmosphere has been established primarily by observations using radar (e.g. Browning 1971). Such billows, with wavelengths up to 5 km and vertical depths of the order of 1 km, have been considered mainly as a concern to aviation safety by causing clear air turbulence (CAT). However, billows also mix across their depth and dissipate kinetic energy (Bryant and Browning 1975; Kennedy and Shapiro 1980), so they could have a significant effect on the larger scale features in which they are embedded, such as a jet stream or frontal zone.

Billows observed in the atmosphere (for examples, see Gossard 1990) occur across layers of stratified shear and tend to have a structure very similar to that found in laboratory tank experiments (Thorpe 1973, 1987) and numerical models (Sykes and Lewellen 1982; Scinocca 1995; Fritts *et al.* 1996a) of the Kelvin–Helmholtz instability (e.g. Drazin and Reid 1981; Readings 1973). This instability occurs when a stably stratified transition layer between two fluids of different density is rolled up by a shear across the layer, forming billows orientated such that their axes lie at right angles to the shear. The stability of the layer is governed by the Richardson number, Ri , defined by N^2/S^2 when N is the Brunt–Väisälä frequency, and S is the vertical wind shear. A necessary, but not sufficient condition for instability is that $Ri < \frac{1}{4}$ somewhere in the flow (Miles and Howard 1964). Although the exact criterion depends on the profiles

* Corresponding author: Joint Centre for Mesoscale Meteorology, Department of Meteorology, University of Reading, Whiteknights Road, PO Box 243, Reading, Berkshire RG6 6BB, UK. (The Joint Centre for Mesoscale Meteorology is supported by the Meteorological Office and the Department of Meteorology, University of Reading, and by the Natural Environment Research Council through its support of the Universities Weather Research Network.)

of N and S , in practice the atmosphere will be unstable if Ri falls much below $\frac{1}{4}$. Observations using high-power radar which detects regions of high refractive index variance to delineate billows occurring in clear air, show that billows occur where $Ri \approx \frac{1}{4}$ (e.g. Browning 1971). The value of Ri depends critically on the depth of the layer over which it is measured and so it is significant that the measurements by Browning were for large-amplitude billows which occurred over depths large enough to be resolved by the radiosondes used.

This paper builds on an initial study by Chapman and Browning (1997) (hereafter referred to as CB), and addresses two questions regarding large-amplitude billows in the atmosphere. Firstly, what causes large-amplitude billows to occur where they do? Roach (1970), Bosart and Garcia (1974) and Keller (1990) have attempted, with mixed success, to relate areas containing billows and CAT to indices diagnosed from larger-scale properties of the flow in the upper troposphere. Billows may also occur due to vertically propagating gravity waves breaking at their critical level (e.g. Fritts *et al.* 1996b), possibly in a location related to the orography. Here we suggest that, in addition to these locations, billows may be a fairly common (but largely unobserved) feature of surface warm fronts.

The second question is what is the meteorological significance, i.e. up-scale effect, of the billows? Although the relevance to aviation safety has been established (e.g. Knox 1997), their direct effect on atmospheric profiles through vertical fluxes of temperature and momentum has been measured to any significant extent only within, or at the top of, the boundary layer (e.g. Metcalf and Atlas 1973; Blumen 1984), where billows generally have a smaller wavelength and depth. In this study, the availability of high-resolution Doppler radar data through billows has allowed the three-dimensional flow field to be calculated, which has in turn yielded vertical fluxes of momentum. Although the flux estimates are subject to considerable error, they nevertheless imply a change in the vertical profile of wind velocity that is consistent with the change directly observed between upstream and downstream of the billows. This suggests that the method described for calculating momentum flux profiles may be useful if a suitable dataset were to be acquired in the future.

We shall show that the role of moisture at the front is important, both in causing billows to occur, and in enabling them to have a large depth (comparable with the depth of the frontal zone itself). Thus large-amplitude billows may cause considerable vertical mixing within a significant proportion of warm fronts, and this mixing may itself substantially alter the structure of the frontal zone. This case study demonstrates the existence of a latent shearing instability, which is released when a layer is lifted to saturation. We refer to this as potential shearing instability (PSHI).

2. THE NATURE OF THE BILLOWS AND THE RADAR DATA

(a) *The Chilbolton radar*

Observations were made using the 3 GHz multi-parameter radar (Goddard *et al.* 1994) at Chilbolton (51.15°N, 1.44°W) which is approximately 80 km north of the south coast of England. The radar has a peak power of 560 kW, and has Doppler capability, allowing the radial velocity of the target echoes to be measured to an accuracy of around 0.1 m s^{-1} . The observations were made within light precipitation and this enabled the billows to be detected at longer ranges than is possible in the clear air. The data have a range resolution of 300 m which is achieved by range-averaging over groups of four gates, each 75 m in length. The dish is 25 m in diameter, giving an angular resolution

of 0.28° . This is an unusually high angular resolution for a 10 cm wavelength radar. It allows the presence of billows similar to those described below to be identified (given precipitation to render them detectable) out to a range of around 80 km, although the data beyond a range of around 50 km do not resolve much quantitative information on the structure of billows.

(b) *General properties of the radar data collected within billows*

Data were collected continuously during the passage of a strong warm frontal zone, between 1600 and 2300 UTC on 6 September 1995. The data were in the form of both RHIs (range height indicators) and PPIs (plan position indicators). In RHIs the radar beam is scanned at different elevations in a fixed bearing (azimuth)—equivalent to a cross-section through the atmosphere in a vertical plane passing through the radar. The RHIs used in this study each took between 15 and 20 seconds to complete, which is negligible compared to the time-scales of the processes of interest. In PPIs the radar beam is scanned in azimuth at a fixed (normally low) elevation. Decisions concerning where to scan were made as the data were acquired, depending on the nature of the data at the time, rather than following a predetermined pattern of RHIs and PPIs.

When the radar is scanned at low elevations the Doppler velocity of precipitation targets yields the line-of-sight horizontal wind component, essentially uncontaminated by the vertical fall-speed of the precipitation (the majority of the data used were from elevations below 5° ; at this elevation the error is around 0.5 m s^{-1} , although this is a somewhat systematic effect). Thus the air motion within the frontal zone and associated billows can be seen clearly in the Doppler data. The billows also appeared to induce small drizzle shower clouds in a convectively unstable region which existed just above the frontal layer containing the billows (refer ahead to Fig. 8(a) for evidence of potential instability). These showers then produced weak reflectivity cores orientated parallel to the billows, but travelling at the velocity of air above the shear layer, so moving out of phase with the billows. For the purposes of this study, all further discussion of the Chilbolton radar data will refer only to the strongly sheared warm frontal zone rather than the overlying convection, and to the Doppler data as opposed to the reflectivity data.

Billows were observed in the radar data between 2005 and 2050 UTC when scans were made at intervals of 5° between azimuths 210° and 270° , and again between 2200 and 2240 UTC when scans were made between azimuths 0° and 90° . The data obtained in the latter period are particularly useful as they include RHIs which were orientated perpendicular to the axes of the billows, although no PPIs were obtained over this period. Between these two periods scans were made in all general directions but only at ranges greater than 50 km, and no billows were observed, although billows are presumed to have continued to exist during this interval but to have been unobserved because of the ranges scanned.

The billows were orientated with their axes almost due south–north. Examples of RHIs orientated at right angles to their axes (i.e. at an azimuth of 90°) are shown in Fig. 1(a)–(c). In addition to the field of Doppler velocity (a), two derived fields are shown. These are (b) the vertical wind shear, clearly showing the structure and extent of the billows, and (c) a streamfunction which indicates air parcel streamlines projected onto the plane of the diagram. These have been derived by integrating the continuity equation upwards from the ground, making the assumption that there is no significant variation of the south–north component of velocity in the south–north direction (for

more details see CB). Labels on the closed stream function contours indicate the time taken in minutes for air parcels to complete a circuit, assuming the circulation remains roughly constant. Figures 1(d) and (e) show an example of similar billows observed in another warm frontal zone on 11 February 1997. This case will be discussed further in section 5(d), but most of the paper will deal with the September case (Figs. 1(a)–(e)) previously studied by CB.

A schematic diagram showing the location and orientation of billows relative to the front with which they were associated is shown in Fig. 2 (quantitative aspects are discussed later). The locations of billow ‘crests’ were determined subjectively from peaks of Doppler velocity in RHIs such as Fig. 1(a). The surface front itself, as defined by sharp gradients in the wind field from radar observations, moved northwards at around 10 m s^{-1} . As this figure indicates, the radar was capable of resolving the billows well only at close range, as they passed close to the radar site. It seems likely that billows existed along other parts of the front (in a strip moving with the surface front, continuing beyond the range of the radar) and also at earlier times, when this strip was beyond the range of the radar. Owing to the nature of the air flow within the billows, they are most evident in the Doppler data when observations are made perpendicular to their axes. There is no Doppler evidence of them when observations are made along their length.

A hodograph derived from two Doppler velocity RHIs separated by 45° within the billows (averaged over two billow wavelengths) was shown in Fig. 3 of CB. The main features of the hodograph are represented by the two vectors shown in Fig. 2 of the present paper. The billows were orientated perpendicular to the main shear between 0.4 and 1.6 km. There was a mean southerly wind of around 20 m s^{-1} at the height of the billows and since the billow train was travelling northwards with the warm frontal zone at 10 m s^{-1} , the component of flow within the billows along their axes was at a relative speed of 10 m s^{-1} . Thus the closed streamlines in Fig. 1(c) represent approximately helical air-parcel trajectories in the core of the billows. The time taken for an air parcel to complete a circuit (i.e. for the air to completely overturn) within the billows was approximately 20 minutes, assuming that the streamlines shown are representative of the billows along all their length.

East–west scans were made by the radar as the train of billows advanced northwards, towards and then over the radar site. Just before the billows reached the radar, the observations were therefore just downwind (north) of the billows. Later (e.g. Fig. 1(a)), while the train of billows was above the radar, observations were made within the billows themselves. The vertical extent of the layer containing a positive west–east component of shear (averaged over an integral number of wavelengths) was 0.4 to 1.7 km within, and 0.5 to 2.5 km just downwind of the billows. Their wavelength was between 4 and 5 km. There was considerable variation in the along-axis length of the billows, ranging from around 10 to 40 km. An accurate measurement of the mean length could not be made, as many of the billows lay partly outside the region scanned by the radar, but a subjective estimation of around 30 km is reasonable. The train of billows as a whole had a south–north extent slightly greater, around 40 km, due to variation in the location of individual billows. The overall train of billows existed for all the time that the radar was capable of observing them (3 hours). This is considerably longer than the residence time of air parcels within individual billows which, since the air was moving along their axes at a relative speed of 10 m s^{-1} , was around 50 minutes. Browning and Watkins (1970) observed billows of a similar amplitude complete their lifecycle over a period of 10 minutes. Evidently the larger-scale flow was acting to sustain the shearing instability over a longer period in the present study.

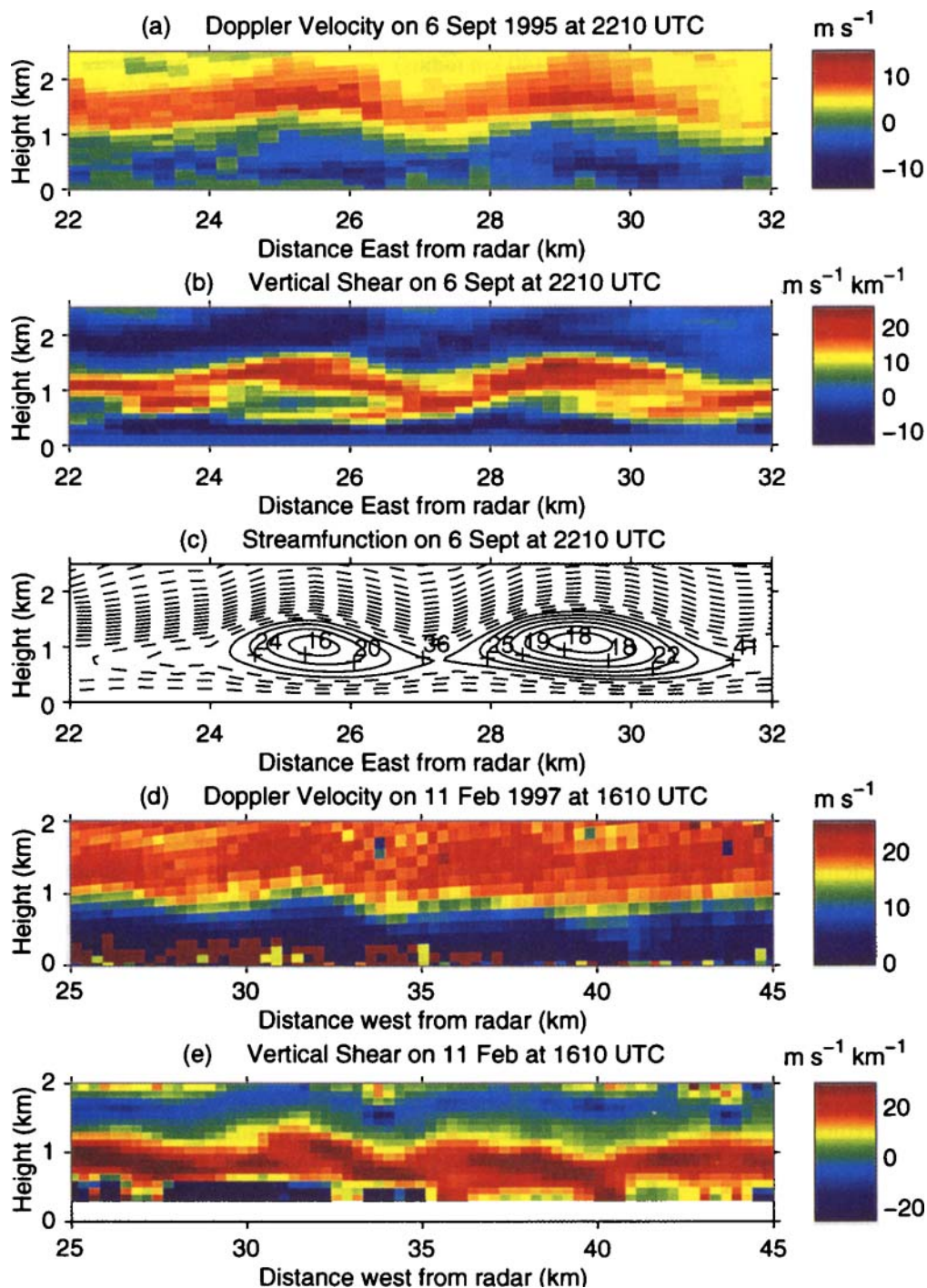


Figure 1. (a)–(c): Range height indicators (RHIs) obtained at 2210 UTC on 6 September 1995 at an azimuth of 90° through billows showing (a) Doppler velocity, giving u (m s^{-1}), positive values indicating air flow to the east, (b) vertical shear, $\partial u/\partial z$ ($\text{m s}^{-1} \text{ km}^{-1}$) and (c) mass-weighted stream function (intervals of $500 \text{ kg m}^{-1} \text{ s}^{-1}$) indicating parcel streamlines in this plane; details are discussed in the text. (d) and (e) show the Doppler velocity and vertical shear through billows observed at 1610 UTC on 11 February 1997. The patterns in the latter two RHIs are not as clear as in the first three because scans could not be made exactly perpendicular to the billow axes.

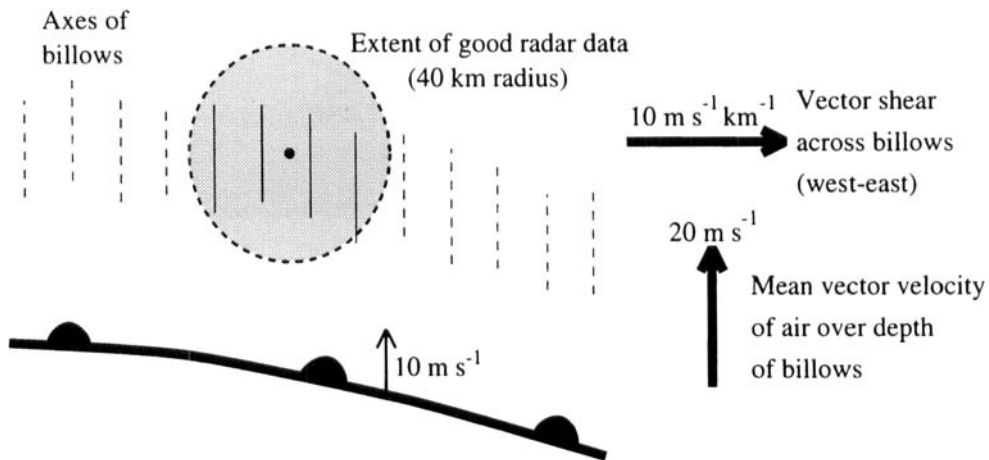


Figure 2. Schematic diagram showing the extent of radar coverage, the observed location of billow axes (shown by solid lines) and the likely location of the billows (dashed lines) in relation to the surface warm front.

3. USE OF MESOSCALE MODEL TO DETERMINE ROLE OF MESOSCALE STRUCTURE IN DETERMINING LOCATION OF BILLOWS

(a) *The mesoscale model*

The version of unified model (UM) used here is essentially as described by Cullen (1993). To summarize, the mesoscale version of the model, which is nested inside the limited-area model, uses a hybrid vertical coordinate which is terrain-following in the lower layers of the atmosphere. It has 31 levels in the vertical, with a resolution of around 60 m at the surface, and 350 m at an altitude of 2 km. A regular latitude-longitude grid is used in the horizontal, with a resolution of 0.15° (corresponding to approximately 16.8 km). It takes its lateral boundary conditions from the coarser-resolution limited-area model in which it is nested. Below about 2.2 km, vertical transport of quantities is implemented by a diffusivity which is dependent on the height above ground, surface roughness, local static stability and shear (and thus the local Richardson number) (P. Clark, personal communication). These transports are calculated taking into account the presence or absence of cloud and thus the effect of latent heat release on the static stability. The billows described in this paper occurred at the top of, and partly within, this layer which will have been subject to some vertical diffusion as described above. Nevertheless, the amount of diffusion in the model will have been calculated making the assumption that the eddy scales were determined by the proximity of the ground, so the model will have greatly underestimated the mixing that actually occurred. Above approximately 2.2 km there is no such calculation, and no artificial vertical diffusion is explicitly imposed (other than that resulting from the numerical schemes used in the model).

The data used in this study come from the 1800 UTC operational run of the model on 6 September 1995. As comparisons between the model and observations are made at 2200 UTC, this allows the model 4 hours to 'spin up' to give a realistic representation of the atmosphere.

(b) *The warm frontal structure as determined by the mesoscale model*

A plan view showing the mean sea-level pressure and the analysed surface warm front (SWF) at 2200 UTC is given in Fig. 3. This figure also shows the location of south-north cross-sections of model data centered on the Chilbolton radar which are given

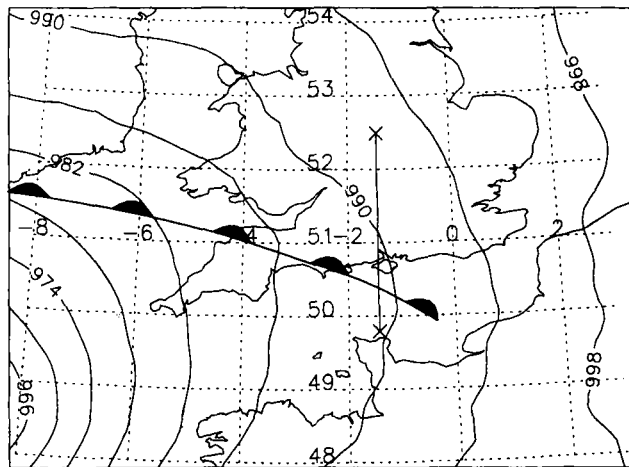


Figure 3. Mean sea-level pressure and the analysed position of the surface warm front from a 4-hour forecast by the mesoscale model, valid at 2200 UTC, 6 September 1995. XX shows the position of the cross-sections in Fig. 4.

in Fig. 4(a)–(d). These show details of wet bulb potential temperature (θ_w), relative humidity (RH), west–east component of the wind (u), and front-relative wind arrows projected onto this section. They indicate the following features of the front:

- Warm, moist air approached the SWF at low levels (below 1 km) from the south, and then rode up over the frontal zone, retaining an eastward component as it did so.
- Cold, and initially dry air ahead of the surface warm frontal zone travelled westwards, approaching it at low levels. As it entered the lower part of the frontal zone, it rose and then moved northwards retaining its westward component as it did so.
- Air within the frontal zone itself originated mainly from the boundary layer just ahead of the SWF.
- The warm and cold air had a relative motion that was broadly consistent with the thermal wind relation, so the change from an easterly to westerly component with height just north of the SWF was related to the temperature gradient across the front.

An upper cold front (UCF) existed ahead of the SWF, with banding in the cloud and precipitation similar to that described by Browning *et al.* (1973b). Behind the UCF the dry, low- θ_w air overriding the moist warm-sector air gave rise to potential instability. The convective cells referred to earlier were due to the release of this potential instability (Chapman 1998), but this is incidental to the main theme of the paper.

(c) *Validation of the larger-scale thermodynamic features reproduced by the model*

Figure 5 shows time–height plots of θ_w , from (a) the mesoscale model and (b) radiosonde data from Herstmonceaux (the nearest radiosonde station with reasonable temporal and height coverage on this date), both at 0.3°E, 50.9°N, 120 km to the east of the sections in Fig. 5. Warm air is shown shaded in the section from the model. The two sections show good agreement in the following respects:

- The SWF passes over Herstmonceaux at the same time (0200 UTC \pm 1 h).
- θ_w at the SWF is within 0.5 K of 288.5 K.
- The ascent at 2000 UTC gives a similar depth between 287 and 289 K through the front, although the layer between these two temperatures in the model is slightly higher and deeper.

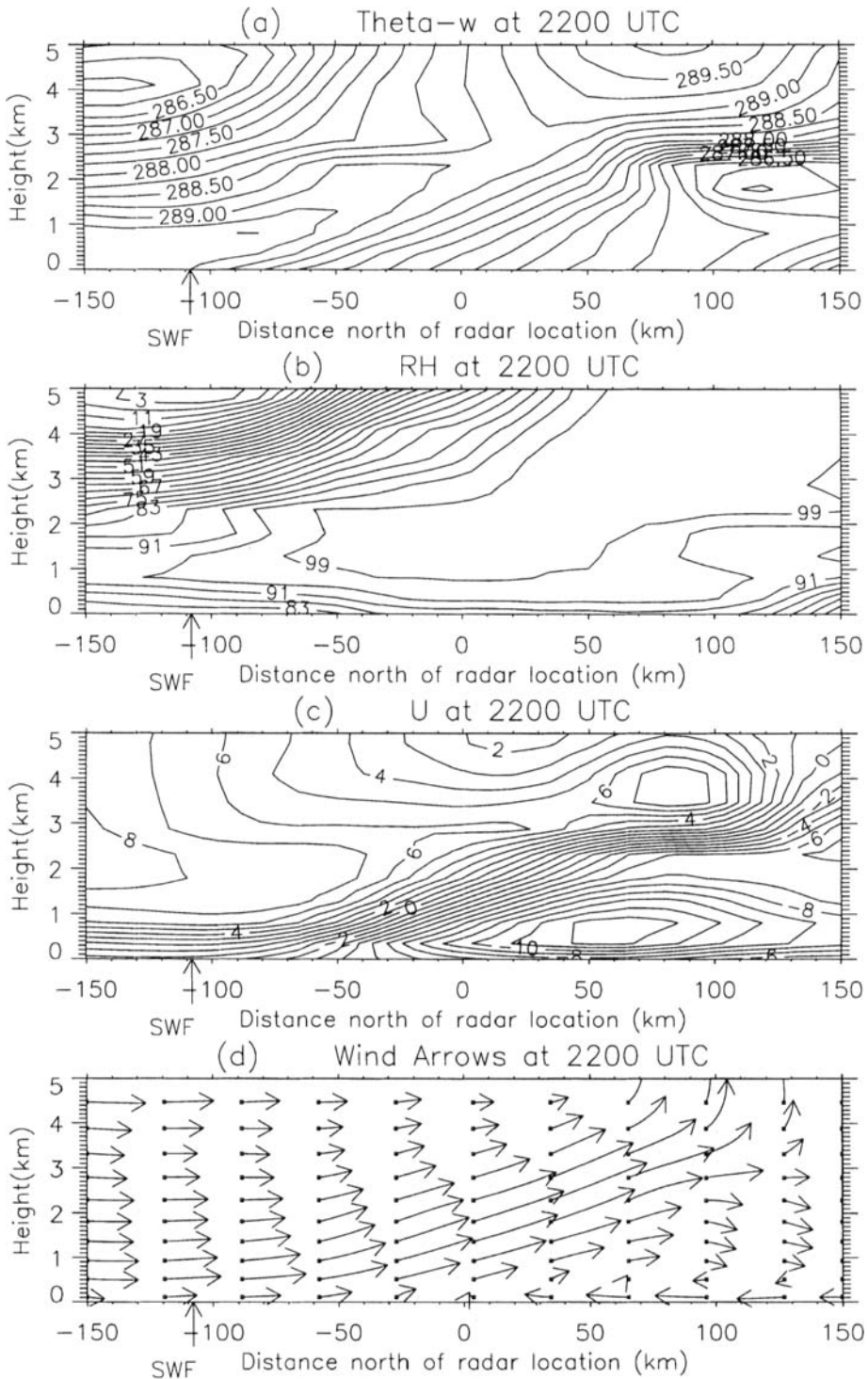


Figure 4. Vertical cross-sections from the mesoscale model at 2200 UTC, 6 September 1995 along the line XX in Fig. 3 which passes through Chilbolton radar. (a): Wet-bulb potential temperature, θ_w (K). (b): Relative humidity with respect to ice (%). (c): West-east component of the wind, u (m s^{-1} , +ve out of the plane). (d): Front-relative wind arrows, the length of each indicating parcel displacements over a period of 1 hour. SWF is the position of the surface warm front.

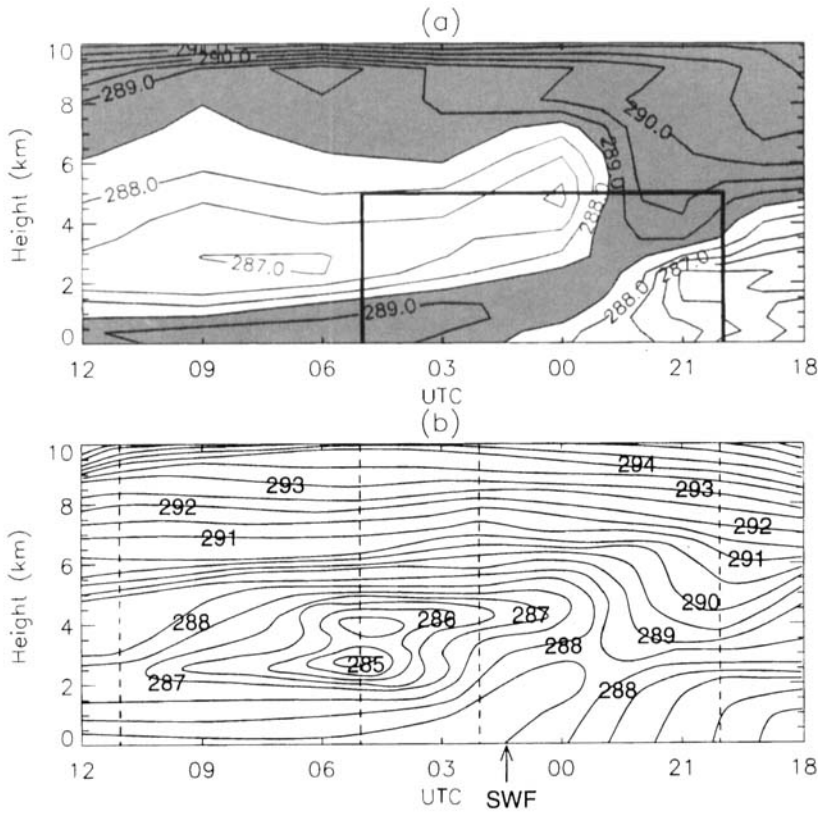


Figure 5. Time–height sections of wet bulb potential temperature, θ_w , above Herstmonceaux on 6/7 September 1995, derived from (a) mesoscale model and (b) radiosonde ascents. The warm air ($\theta_w > 288.5$ K) is shown shaded in (a). The times of radiosonde ascents are indicated by the dashed lines in (b). Owing to the sparsity of data in some regions of (b) the mesoscale model has been used to help interpolate the radiosonde data in a realistic way (although the contours still fit the radiosonde data at the times of ascents). The equivalent location of distance–height cross-sections in Figs. 4, 6 and 8 is shown by the rectangle in (a).

Thus the model is interpreted as having reproduced actual thermodynamic structures well, locating them to within around ± 90 minutes. This corresponds to a distance of approximately 55 km, which is 3 model grid lengths.

(d) *The model’s detailed representation of the frontal zone and the adjustments required to fit the observations*

Section 3(c) has demonstrated that the model and the observations were broadly consistent. However, in order to relate the radar observations of the billows to the model we need to obtain consistency on smaller scales of order 10 km. The aim of this section is to show how the model, which yields both thermodynamic and kinematic fields, has been adjusted slightly so that it is consistent on these scales with the kinematic fields obtained from the radar, and other observations. This adjustment has been done to obtain the ‘best estimate’ of the state of the atmosphere at the exact time and place where the billows are known to have existed.

(i) *Comparison of the model’s southerly wind component (v) with that measured by the radar.* Figure 6 shows a cross-section of the southerly (front-normal) component of wind from the model and radar at 2200 UTC. The main feature is the low-level ‘jet’

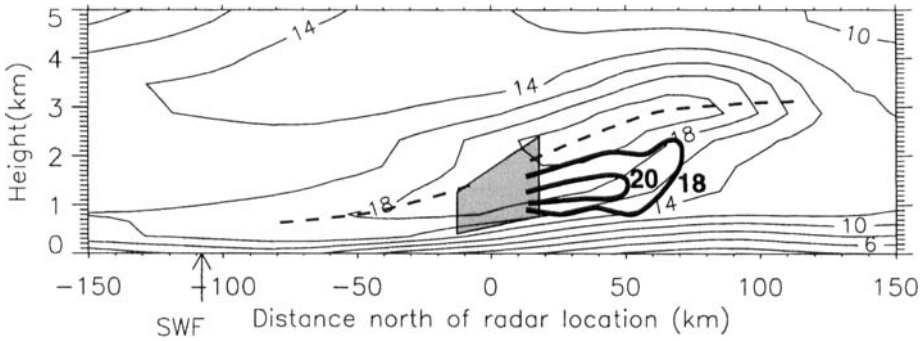


Figure 6. South–north cross-section at 2200 UTC, 6 September 1995, along the line XX in Fig. 3 showing the southerly component of wind, v (m s^{-1}) from the mesoscale model (thin lines). The model's jet axis is shown dashed. Superimposed are two contours (18 and 20 m s^{-1}) of the same component of the wind measured by the radar (bold lines). The radar-detected location of the billows is shown shaded.

of warm air which rides up over the frontal zone. In the model and radar data, this jet has a similar shape, slope and magnitude, with a maximum of around 20 m s^{-1} . However, the location of the jet axis is displaced in the model relative to the radar. This displacement could be due to the model having located the frontal system (A) too far south by approximately 40 km, or (B) too high by approximately 800 m, or a combination of (A) and (B). Evidence given below in section 3(d)(ii) suggests that (A) is more likely. The apparent discrepancy in the location of the northern end of the jet axis that would be introduced by assumption (A) may be explained by the inadequacy of the vertical mixing in the model, which in reality would tend to weaken the jet over the length of the billows which were observed.

(ii) *Comparison of the model's westerly component of the wind shear ($\partial u/\partial z$) with that measured by the radar.* We compare in Fig. 7 the wind shear profile ($\partial u/\partial z$) derived from radar data within the billows with the two corresponding model wind shear profiles derived assuming (A) and (B) above, respectively. A comparison has been made of the height of the maximum in the shear profiles because of its insensitivity to the effect of the billows (which is to diffuse the shear in the vertical, without changing the height of the maximum shear). The radar observations (Fig. 7(c)) show a maximum in the vertical wind shear at a height of 1.2 km. The corresponding maximum occurs at heights of 0.8 km and 0.5 km in Figs. 7(a) and (b) respectively. The closer fit of (a) supports assumption (A), implying that the model mis-located the front by around 40 km to the south. This is consistent with the resolution of the model, as a displacement of 40 km horizontally implies an error of only about 2 grid lengths. In contrast, there are 4 model levels between 0.5 and 1.2 km, so a vertical error as large as 700 m seems less appropriate in any case.

In addition, the shear layer responsible for the billows was spread out over a greater depth in the model. As a consequence, the peak shear was only around $10 \text{ m s}^{-1} \text{ km}^{-1}$ in the model (Fig. 7(a)) compared to $14 \text{ m s}^{-1} \text{ km}^{-1}$ in the profile derived from the radar data (Fig. 7(c)).

(iii) *Comparison of the model's relative humidity with observations from synoptic reporting stations.* As we shall see later, the behaviour of the billows depended critically on the level of saturation (i.e. the height of the cloud base) and so it is important to adjust any small errors that there may have been in the model's relative humidity field,

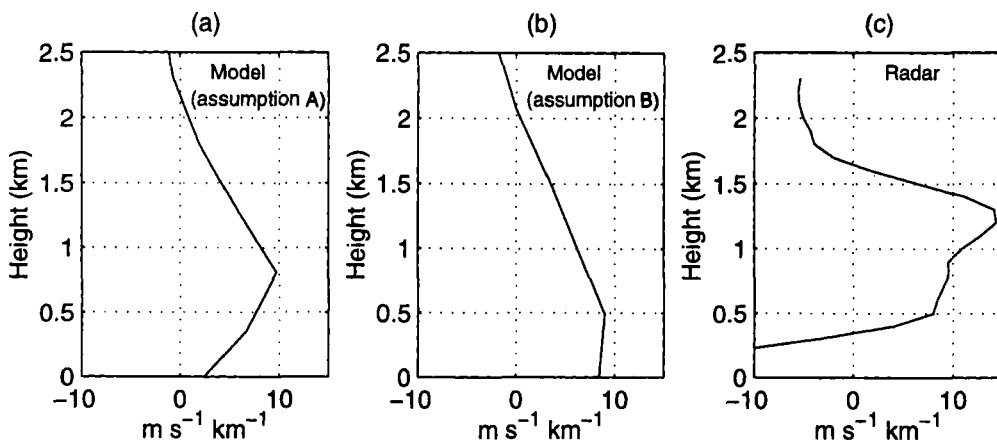


Figure 7. Vertical profiles of the westerly component of the vertical wind shear ($\partial u/\partial z$) at 2200 UTC, 6 September 1995, in the region of the billows. (a) and (b): Model-derived profiles obtained after adjusting the model according to assumptions (A) and (B), respectively (see text). (c): Radar-derived profile based on radar data averaged over times 2200, 2210 and 2220 UTC, and averaged over 12 km close to the radar.

especially at low levels where the billows occurred. The model cross-section showing RH in Fig. 4(c) indicates a cloud base, assuming that this is given by the 99% contour, at around 900 m. However, synoptic observations at this time indicate that the cloud base north of the SWF was lower than this, at approximately 400 m.

(iv) *Adjustment of the model fields.* Section 3(c) has validated the model on scales greater than 100 km horizontally, and 500 m vertically. The comparisons made in sections 3(d)(ii) and 3(d)(iii) indicate the need for all of the following finer scale adjustments:

- displace all model fields 40 km north to agree with Doppler radar observations of the kinematic structure of the front,
- increase model shear by a factor of 1.4 in the frontal zone, to agree with radar observations of the shear responsible for the billows,
- reduce height of $RH = 99\%$ contour by 500 m to around 400 m, to agree with cloud base observations.

By adjusting the model output in this way, the resulting fields will be more accurate (though less balanced) than the raw model fields, and of course much more comprehensive than the actual observations. The discrepancy that is introduced in the location of the northern end of the south–north jet may be explained as the result of the mixing induced by the billows not being represented by the model.

Figure 8(a) shows the resulting adjusted model fields of θ_w and $RH = 99\%$ in the region of the surface warm front, including the location of the observed billows and the front-relative airflow into them. The causal relationship between these fields and the location of the billows will be discussed in section 3(f).

(e) *Calculation of the Richardson number*

The Richardson number is defined as the ratio of the static stability to the square of the vertical wind shear. However, in this case the evaluation of Ri appropriate to the billow formation is complicated by two factors: (i) the proximity of the frontal shear zone to the strong differently orientated shear in the boundary layer, and (ii) the saturation of much of the frontal zone.

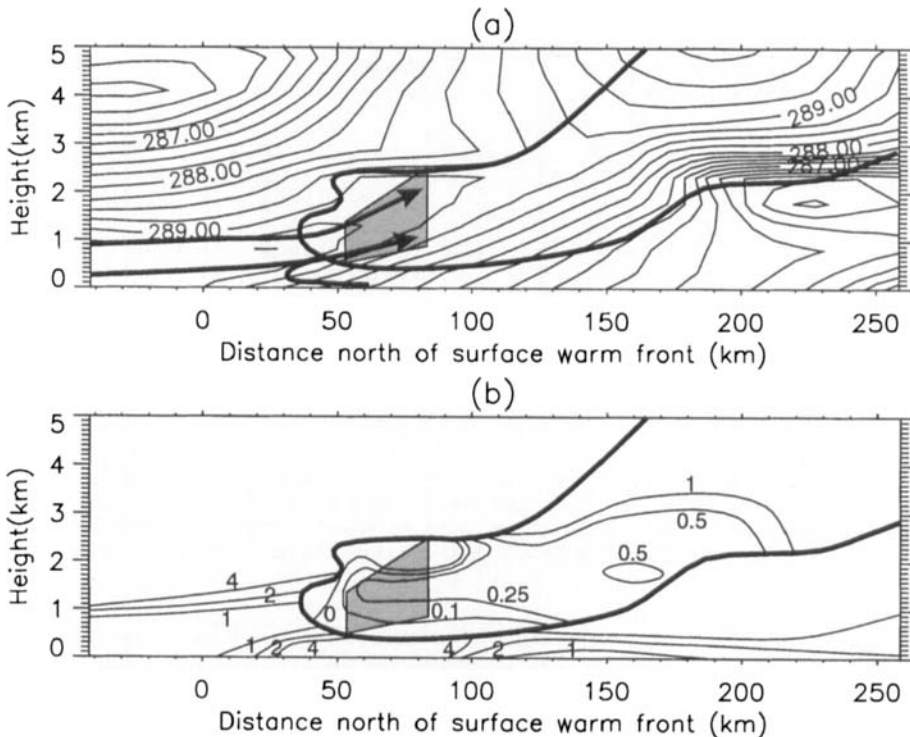


Figure 8. South–north vertical cross-sections (passing through Chilbolton radar) at 2200 UTC, 6 September 1995, showing fields adjusted as described in the text. The fields shown are (a) wet-bulb potential temperature and front relative streamlines entering the region containing the billows and (b) Richardson number Ri as defined in section 3(e). The effective region of saturation ($RH > 99\%$) is delineated by a bold contour, and the radar-detected location of the billows is shown shaded, in both (a) and (b).

(i) *The problem of the variable orientation of the shear vector.* The hodograph shown in Fig. 3 of CB indicates that there was a strong south–north component of wind shear between the ground and a height of 0.6 km, which would have been associated with relatively small-scale turbulent mixing in the boundary layer. The strong west–east component of shear responsible for the observed large-amplitude billows existed between 0.4 and 1.6 km. Although the lower portion of the billow shear layer, between 0.4 and 0.6 km, slightly overlapped with the boundary-layer induced shear, most of the billow layer, between 0.6 and 1.6 km, was characterized by an almost zero component of shear in the south–north direction. The south–north component of the wind shear has been neglected in the following calculations of Ri since it is only the instability of the flow to large-amplitude billows that we are concerned with in this study. By calculating Ri in this way we greatly increase the apparent Richardson number in the boundary layer, but the value in the frontal zone is close to the actual Richardson number because of the very small south–north component of shear over the layer containing billows.

(ii) *The effect of saturation on the static stability.* Where the air is unsaturated ($RH < 99\%$) the static stability has been defined as

$$N^2 = N_d^2 = \frac{g}{T} \left(\frac{dT}{dz} - \Gamma_{dry} \right) = \frac{g}{\theta} \frac{d\theta}{dz} \quad (1)$$

where g is the gravitational acceleration, T and θ are the sensible and potential temperatures of the atmosphere, and Γ_{dry} is the dry adiabatic lapse rate. However, for a given temperature profile, the atmosphere will always have a reduced static stability if it is made saturated, due respectively to the release and absorption of latent heat accompanying upward and downward air-parcel displacements. Although for large vertical displacements the evaporation of water droplets may be too slow to maintain saturation, it is reasonable to assume that, in the early stages of the growth of an instability, small downward displacements by an air parcel can maintain saturation by rapid evaporation of the smallest cloud droplets. In regions where the air is saturated ($RH > 99\%$) the static stability has been defined as (Lalas and Einaudi 1974)

$$N^2 = N_w^2 - \frac{g}{T} \left(\frac{dT}{dz} - \Gamma_{sat} \right) \left(1 + \frac{Lq_s}{RT} \right) - \frac{g}{1 + q_w} \frac{dq_w}{dz} \quad (2)$$

where L is the latent heat of evaporation, R is the gas constant, q_s is the saturation mixing ratio, q_w is the total water mixing ratio and Γ_{sat} is the saturated adiabatic lapse rate. This expression for N_w^2 was shown by Durran and Klemp (1982) to be a good approximation to the correct value, and a much better approximation than that obtained by a simple substitution of θ_w for θ in (1).

Ri was calculated at 50 mb intervals, over depths of 100 mb (corresponding to a height interval of around 800 m), which is comparable to the observed depth of the billows. The result is shown in Fig. 8(b). The different definitions of N^2 in the saturated and unsaturated regions lead to discontinuities at the cloud boundary.

(f) *The aspects of the mesoscale frontal structure that determined the location of billows*

Figure 8 shows the best estimate of the relevant thermodynamic and kinematic fields in the frontal zone at the time of the billows. The processes leading to the development of the billows can be inferred from these fields.

High- θ_w air which approached the frontal zone from behind (i.e. south of) the surface front (upper bold arrow in Fig. 8(a)) was initially unsaturated. Ascent occurred in association with convergence near the surface front, and above 400 m the air became saturated as it flowed northwards. Lower- θ_w air which approached the frontal zone at low levels (in the boundary layer) from the north was also unsaturated. Close to the surface front, this air mixed with warmer air and then it too ascended (lower bold arrow in Fig. 8(a)), becoming saturated as it travelled upward and northward conserving its θ_w .

These two air-streams, represented by the two bold arrows in Fig. 8(a), were in relative motion in the direction perpendicular to the cross-section, broadly in agreement with the thermal wind relation. This gave rise to the strong shear layer between them. This is the shear layer that caused the large-amplitude billows to occur. If the air had been dry, then the sheared layer would have had a minimum Richardson number of around 1 over a depth of 800 m. However, the air was saturated, and so the layer had a Richardson number of between 0 and $\frac{1}{4}$ when measured over 800 m increments (Fig. 8(b)), consistent with the observed occurrence of large-amplitude billows.

The location of initiation of billows in the frontal region, according to the analysis, was dictated by the height of the $RH = 99\%$ contour (although the height of this contour itself may in turn have been affected to some extent by the presence of the billows). Upstream of the billows, while the flow was still unsaturated, the shear was allowed to become large whilst the dry Richardson number remained well above $\frac{1}{4}$. The Richardson number when calculated assuming the air was saturated in this location was, however,

less than $\frac{1}{4}$. This potential for instability was then released 'immediately' the air became saturated, initiating billows over a considerable vertical depth of 1 km, with an initial minimum Richardson number well below $\frac{1}{4}$.

4. THE EFFECT OF THE BILLOWS ON THE MESOSCALE FRONTAL STRUCTURE

(a) Introduction

The Doppler radar wind profiles within and downwind of the billows showed a considerable change over a south–north distance of around 30 km (see Figs. 5(a) and 5(b) in CB). Part of this change was due to the lifting of the overall frontal shear layer with distance ahead of the surface front. The other part of the change was due to the shear over the layer containing billows being redistributed over a greater depth. Although the nature of the change is consistent with it having been caused by the billows, it could alternatively be a feature of the larger-scale flow field. In section 4(b), estimates are presented of the vertical profiles of the vertical flux of horizontal momentum due to the resolvable flow patterns associated with the large-amplitude billows. Although the estimates are prone to considerable error and do not constitute an adequate statistical sample, they tend to support the view that the billows themselves could have been responsible for the observed change in the wind profile over their length.

(b) Calculation of momentum flux from radar measurements

The Reynolds decomposition for data from point measurements is performed by separating fields into their time-mean and time-dependent parts, such that the time-scales of the two parts are widely separated (e.g. Stull 1988). However, in the present case, the data are in the form of spatial fields of the front-parallel (i.e. west–east) component of the wind, u , and the vertical wind velocity, w , so the measurements are separated instead into their horizontal-mean (denoted by angled brackets) and horizontal-dependent (denoted by asterisk superscript) parts:

$$u = \langle u \rangle + u^* \quad w = \langle w \rangle + w^*$$

where the mean is taken over an integral number of billows wavelengths.

When this decomposition is incorporated into the equations of motion, the term representing the effect of the billows on the mean flow is given by the Reynolds stress component in the front-parallel (x) direction, $-\rho \langle u^* w^* \rangle$ (ρ being the density of air), which is the component of the momentum flux due to the billows. The effect of the billows on the mean flow is given by the momentum flux convergence, so

$$\frac{D\langle u \rangle}{Dt} = -\frac{\partial \langle u^* w^* \rangle}{\partial z} \quad (3)$$

where

$$\frac{D\langle u \rangle}{Dt} = \frac{\partial \langle u \rangle}{\partial t} + \langle v \rangle \frac{\partial \langle u \rangle}{\partial y}.$$

As the vertical scales of motion (around 1 km) are small relative to the density scale-height (8 km), the effect of the variation in density with height has been neglected in the derivation of Eq. 3.

Observations of the billows over three hours indicated that their location remained essentially fixed relative to the surface front, and their structure did not noticeably change. This implies that in a reference frame moving northwards with the front, then

$\partial \langle u \rangle / \partial t = 0$, as long as the mean is obtained over enough billows to eliminate the effect of localized variations in the position of the billows. Thus the term involving momentum fluxes can be directly related to observed changes in wind profiles from north to south:

$$\frac{\partial \langle u \rangle}{\partial y} = - \frac{1}{v_{rel}} \frac{\partial \langle u^* w^* \rangle}{\partial z} \quad (4)$$

where v_{rel} is the southerly component of the wind at the height of the billows relative to the front, equal to 10 m s^{-1} .

At 2210 UTC four billows which existed to the east of the radar were sampled. A plan view of these billows can be seen in Fig. 2 of CB. They were chosen because of their proximity to the radar, and lack of ground clutter in the radar data. These billows will be referred to as I, II, III and IV, from west to east. The Doppler velocity in this direction gives u , directly, and this was interpolated onto a regular grid with spacing 500 m in the horizontal and 100 m in the vertical. This spacing was chosen to correspond broadly to the spatial resolution of the radar data over the ranges used. The vertical velocity, w , was calculated assuming that the billows were two dimensional by integrating the continuity equation (as described in CB) between the ground and 2 km, using a nine-point average around each grid box to smooth the u field. The quantities $\langle u \rangle$ and $\langle w \rangle$, taken as averages of u and w over the four billows between $x = 13.5$ and $x = 31.5$ km, and values of u^* and w^* , were calculated accordingly.

Figure 9 shows the $x - z$ cross-sections of (a) u^* and (b) w^* which were then combined to give (c) $u^* w^*$. The four billows all show the same qualitative structure in each of these fields. Although u^* and w^* vary with the same wavelength as the billows, the field of $u^* w^*$ varies in the horizontal with a wavelength half that of the billow wavelength. For example, over billow IV between 27 and 31.5 km at a height of 1 km, $u^* w^*$ shows a maximum, minimum, maximum then a minimum. There is a further set of maxima and minima at a height of 1.7 km, out of phase with those below. This is consistent with Fig. 13 of Busak and Brümmer (1987) who used a linear analytical model to simulate billows close to the ground. The $u^* w^*$ field was averaged horizontally over each individual billow to give the four mean momentum flux profiles in Fig. 10. As might be expected from Fig. 9(c), profiles from billows I and II are similar to each other, as are profiles from III and IV. However, the latter pair have larger maxima and minima over the depth of the billows, and there is also a displacement in the vertical between the two pairs of profiles, such that the two pairs are approximately in anti-phase with each other. Good quality Doppler data were also available over two other billows (not shown); the momentum flux profiles from these are qualitatively similar to the profiles from I and II.

Only two-dimensional eddies on horizontal scales between around 0.5 and 4 km can contribute to the momentum flux profiles calculated in this way. This is due to the resolution of the radar data and the way the vertical velocity is calculated. Thus it is only the effect of the main overturning of the billow on the mean velocity profile that is being measured, not the effect of its turbulent breakdown by eddies on smaller horizontal scales.

It is likely that a billow going through different stages of evolution would have different momentum flux profiles at each stage, which would account for some of the variation between the flux profiles in Fig. 10. This is supported by the numerical simulations by Fritts *et al.* (1996a), which show that the momentum flux is strongest as the billows grow to maximum amplitude, but then fluctuates with time, even reversing in sign, before it decays to zero. In order to obtain an estimate of the net change in the mean wind profile from upstream to downstream of the billows, all six available

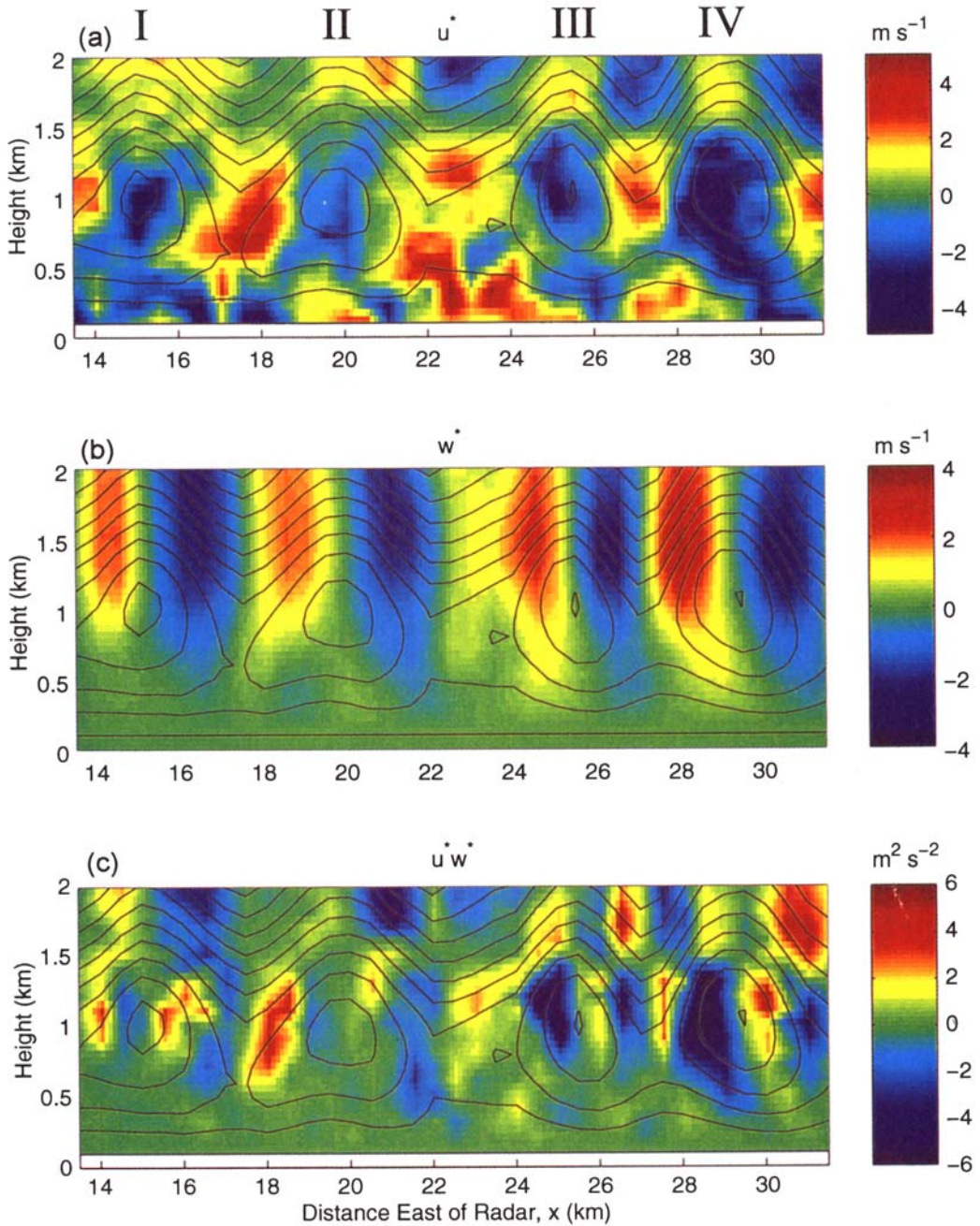


Figure 9. Radar-derived cross-sections through billows east of the radar at 2210 UTC, 6 September 1995, showing stream function (light solid contours) superimposed upon (a) u^* (m s^{-1}) (b) w^* (m s^{-1}) and (c) $u^* w^*$ ($\text{m}^2 \text{s}^{-2}$). Roman numerals refer to individual billows.

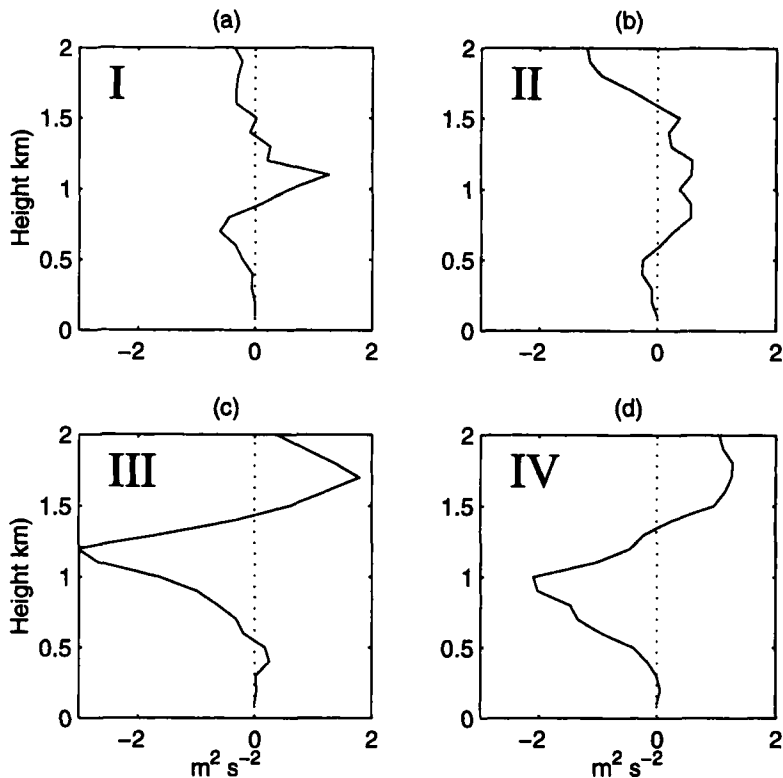


Figure 10. Momentum flux profiles averaged over the individual billows shown in Fig. 9.

momentum flux profiles were averaged. Although it was hoped thereby to sample the billows at six different stages in their evolution, it is not known how well they represent all stages in the evolution and so we have rather low confidence in the representivity of the average profile. The resulting profile is shown in Fig. 11(a), together with a smoothed profile. Smoothing was carried out so that small-scale fluctuations did not dominate in the derivation of the first and second vertical derivatives, as discussed in the following section.

(c) *The effect of the momentum flux convergence on the mean wind shear profile*

According to Eq. 3, the rate of change of the mean wind following the flow is given by the momentum flux convergence. Similarly, the rate of change of the mean wind shear following the flow is given by the vertical derivative of the momentum flux convergence. Averaged profiles of these two quantities, derived from the smoothed profile in Fig. 11(a), are plotted in Figs. 11(b) and 11(c), respectively. Equation 4 has been used to estimate the change in shear profile between locations 5 km south and 5 km north (solid and dashed curves, respectively, in Fig. 12(a)) of the original location of the profile. The shear responsible for the billows initially had a maximum at a height of 1.1 km, and was zero at 1.5 km. At 1.1 km, the vertical derivative of the momentum flux convergence was negative, indicating a tendency for the billows to reduce the peak shear at this height (see arrow in Fig. 12(a)). Between 1.3 and 1.8 km the vertical derivative of the momentum flux convergence was positive, indicating a tendency for the billows to increase the shear, thereby spreading the shear layer out over a greater depth in the

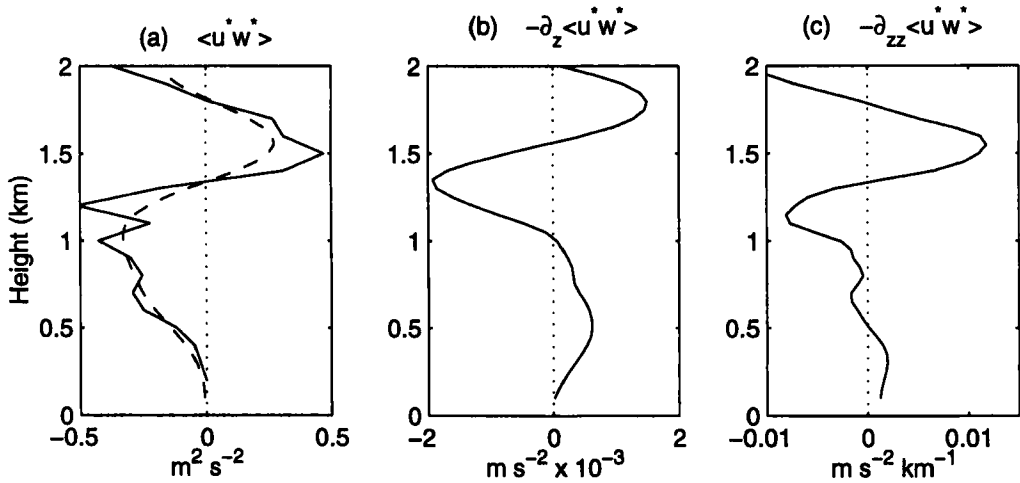


Figure 11. (a): Momentum flux profiles averaged over six billows (see text) east of radar between 2200 and 2220 UTC (solid line). Dashed line is a smoothed fit to the actual data. (b): Momentum flux convergence, derived from smoothed profile in (a). (c): Vertical derivative of the momentum flux convergence, derived from (b).

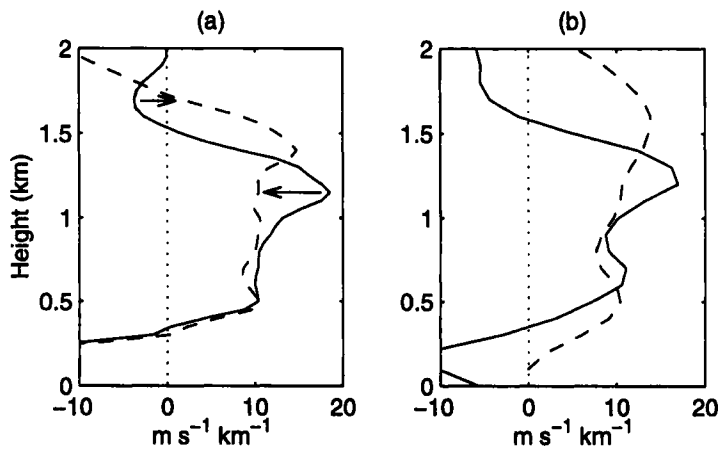


Figure 12. (a): Wind shear profiles at locations 5 km south and 5 km north (solid and dashed curves, respectively) of the initial shear profile, obtained by integrating the profile in Fig. 11(c). (b): Wind shear profiles measured within (solid lines) and downwind (dashed lines) of billows.

vertical. The effect on the shear at lower levels (below 0.5 km) appears to have been considerably less.

(d) *Comparison of calculated and observed profiles of wind shear upwind and downwind of the billows*

Figure 12(b) shows the observed profiles of wind shear at locations towards the southern end (solid curve) and just downwind (dashed curve) of the billows, the two profiles being separated by a distance of around 30 km. This separation is greater than that used above because of the large interval between times when radar scans could be made, as mentioned in section 2(b). The trends in the profiles in Fig. 12(b) are in broad agreement with the trends in profiles inferred from momentum flux calculations (Fig. 12(a)), showing a decrease in peak shear but an increase in shear above 1.4 km, and

a smaller increase below 0.6 km. However, these results should be treated with caution, as there are a number of important sources of error.

The calculation of w is susceptible to inaccuracy in two ways. Firstly, the assumption of non-divergence in the south–north direction may induce a systematic bias in the vertical velocity if this component of divergence is itself influenced by the billows. The nature of the radar data makes it impossible to estimate the magnitude of this effect, although the variation of the south–north component of divergence in the west–east direction is unlikely to have been comparable to the west–east component of divergence itself. Secondly, the vertical velocity field was obtained by integrating upwards from as close to the ground as possible. However, at low levels the radar beam is contaminated by echoes from the ground itself, so the level at which the integration was started (200 m) was relatively high, considering the low altitude of the billows. The effect of errors in w near the ground amplify with height, making this a potentially serious problem. The fields of w obtained are, to some extent, validated by qualitative comparison of the stream function with the original wind field. They also agree with the prediction by Davis and Peltier (1976), that the maximum in the vertical velocity can occur higher than the critical level for the fastest growing instability when the shear layer is close to the ground.

The vertical velocity field which has been calculated represents only the main overturning of the billows, not the small-scale eddies involved in its turbulent breakdown. It is not obvious *a priori* which scale contributes most to the deepening of the shear layer, and how the contribution of each scale varies over the lifetime of the billows. However, three-dimensional numerical simulations by Fritts *et al.* (1996a) indicate that it is mainly the overturning of the billow that affects the mean velocity profile, rather than smaller scale eddies associated with the breakdown of the billow, although these eddies influence the mean profiles indirectly via the evolution of the billow itself. This suggests that the method used here should, in principle, allow measurement of the momentum fluxes responsible for the change in mean shear profile over the lifecycle of billows.

Another source of error is that the sample of six billows is too small to show whether the variation seen in the individual momentum flux profiles is due to variation in the actual billow structure, or due to random errors. Even if the former were true, the sample size would still be too small for a reliable estimate of a representative average momentum flux profile over the lifetime of the billows.

As it happened, the measurements available were through billows that were overturning strongly, probably towards the middle of their lifecycle, so the results support the view that the overturning of the billows may indeed have been responsible for a large part of the observed change in wind shear profile over the length of the billows. The limitations of the present dataset are such that the closeness of the agreement between the momentum flux calculations and the profile changes up- and downwind of the billows is probably fortuitous. The calculations have been done in a way which is analogous to the analysis of data from tower measurements (e.g. Blumen 1984) and aircraft measurements (e.g. Metcalf and Atlas 1973; Busak and Brümmer 1987), i.e. by making averages of correlations over many billows, with no attempt to obtain multiple measurements over an individual billow's lifetime. Any estimate of the momentum flux variance will therefore include the variation of u^*w^* within a billow, as well as random errors and variation in the momentum flux profile over the lifetime of the billows (as shown by Fritts *et al.* 1996a). It is therefore in general very difficult to estimate the uncertainties associated with measurements of momentum fluxes, and studies frequently do not even attempt such an estimate.

Given a future RHI dataset that had been acquired specifically in order to obtain momentum flux estimates over the lifetime of a train of billows, there are two ways in which errors associated with the momentum flux profiles could be estimated:

- Radar RHIs obtained consecutively along the same bearing provide a way of obtaining measurements over a train of billows at intervals of as little as 20 seconds. This is sufficiently short a period (relative to the time-scale for the evolution of a billow) that consecutive momentum flux profiles, calculated over an individual billow, should change very little and certainly remain qualitatively similar. If this were not the case, it would indicate that the assumptions used in the derivation were not valid. On the other hand, a number of consecutive momentum flux profiles, obtained over a time significantly less than the time-scale for the evolution of the billow, would allow a quantitative estimation of the random errors associated with each individual profile. Errors associated with, for example, *localized* departure from 2D flow would, in effect, be random in this context, so their effect on the final profile could be estimated using statistical methods.

- Given validation of the general method as outlined above, individual momentum flux profiles from a single billow could be averaged to obtain a single profile representative of the mixing by that billow over its whole lifetime. This would be possible only if the billow was not advected out of the range of the radar in the time taken for the billow to pass over the radar. Profiles obtained in this way through a number of billows could then be averaged, and an error estimate could be obtained by taking the standard deviation of $\langle u^*w^* \rangle$ at each height. It is clearly not possible to do this with the existing dataset, given its limitations which have already been described.

One additional advantage that this method has over conical scanning radar methods such as that used by Bryant and Browning (1975) is that RHIs will be obtained showing cross-sections through individual billows at various stages in their lifetimes, so variations in the momentum flux profiles may be directly related to the detailed observations of the structure of the billows.

5. FURTHER DISCUSSION AND SIGNIFICANCE OF THE RESULTS

(a) *The possible influence of the proximity of the ground on the nature of the billows*

This paper has described an observational study of large-amplitude billows which occurred over a distance between 50 and 90 km north of a strong surface warm front. The basic parameters describing the billows observed in this study are all consistent with the previous observations and theoretical predictions concerning the Kelvin–Helmholtz instability of a free shear layer (see CB). These parameters include the ratio of the wavelength to the shear layer depth, the orientation and phase speed of the billows, the requirement for Ri to be less than about $\frac{1}{4}$, and indeed the basic structure of the billows, consisting of a train of vortices at the height of the inflexion point in the velocity profile. However, analytical studies (e.g. Lalas and Einaudi 1976; Davis and Peltier 1976) have shown that the close proximity of the ground, as in the case considered, may substantially modify the Kelvin–Helmholtz mode or even allow other resonant modes to exist. The resonant modes are predicted to have a very different structure between the ground and the inflexion point, so are inconsistent with the observations described here. Nevertheless, it does seem likely that the presence of the ground will have affected certain aspects of the billows that were observed, notably the growth-rate (which is predicted to be much reduced when the billows are as close as these were to the ground) and the vertical structure, with the maximum in the vertical

velocity perturbation occurring substantially above the height of the inflexion point. This latter property was observed, and can be seen in Fig. 9(b). However, another possible explanation for this is that the integration to obtain the vertical velocity was unstable in some way, leading to vertical velocity perturbations extending above the height at which the horizontal velocity perturbations became small (around 2.5 km). In any case, it is not felt that the modifications to the billow's structure will have affected the validity of the main conclusions in this paper, although they should be borne in mind when making comparisons with other studies of Kelvin–Helmholtz instability.

(b) *Comparison with other studies of the effect of large-amplitude Kelvin–Helmholtz billows*

There are few published observations of large-amplitude Kelvin–Helmholtz billows in the atmosphere, and even fewer measurements of momentum flux profiles through them. Although the magnitude of the momentum flux will depend on a variety of factors, including the billow size, shear and stage in evolution, it is still worthwhile to compare the results presented in this paper with those from other studies. In one such study Bryant and Browning (1975) used Doppler radar to investigate billows occurring at heights between 1 and 3 km within a warm frontal zone. They used very different methods from those described here to estimate the vertical flux of horizontal momentum. Whereas the billows in the present study had a wavelength of 4 to 5 km, those in the earlier study had a wavelength of 1 to 2 km. The peak shear was about the same in both studies. The magnitude of the resolved momentum flux had a maximum of around $0.1 \text{ m}^2 \text{ s}^{-2}$ in the shear layer, compared with $0.5 \text{ m}^2 \text{ s}^{-2}$ estimated here. This difference is what might be expected in view of the larger wavelength of the billows observed in the present study.

In another study of Kelvin–Helmholtz billows, Blumen (1984) used wind and temperature measurements from an instrumented tower to calculate turbulent momentum fluxes due to billows in two occasions of night-time drainage winds. During periods when billows existed and the wind shear profile was observed to become smoothed with time, then the momentum fluxes acted in such a way as to cause this smoothing. The fluxes had a maximum of around $0.2 \text{ m}^2 \text{ s}^{-2}$ which is less than those calculated here. Again, this would be consistent with the smaller wavelengths (100–200 m) observed by Blumen, although the shear in his case was considerably larger than here.

The momentum fluxes estimated in the present study are of a similar magnitude to those observed in clear-air turbulence at upper levels. For example, Kennedy and Shapiro (1980) found that the magnitude of the momentum flux within a number of upper-level turbulence zones was between around 0 and $4 \text{ m}^2 \text{ s}^{-2}$. Trout and Panofsky (1969) used clear-air turbulence spectra and clear-air turbulence probabilities to show that the dissipation of energy by CAT between 25 000 and 40 000 ft is around 1 W m^{-2} , which is not unimportant in the dynamics of the atmospheric circulation.

(c) *Potential shearing instability and the role of moisture in the formation of large-amplitude Kelvin–Helmholtz billows*

The most robust and important result in this paper is that the large-amplitude billows were observed in a location just north of a surface warm front, which coincided with the onset of saturation due to ascent at the surface front. The onset of saturation suddenly lowered the Richardson number of a deep sheared layer in the frontal zone from around 1 to a value much less than $\frac{1}{4}$. The presence of saturation in the frontal zone was critical in determining not only the location of the billows but probably also the amplitude of the billows that developed. In the absence of the sudden development of instability over

a deep layer due to the onset of saturation, and in the absence of a rapid dynamically-induced increase in shear, it is likely that a critical Richardson number and associated billows would appear first over a shallower layer or layers, leading to initially smaller billows.

The dependence of the dynamic stability of a stratified shear layer on its saturation is analogous to conditional instability (CI), which describes the dependence of the static stability of a parcel on its saturation. A temperature profile exhibits CI at a particular height if the air is statically stable at that height when the air is unsaturated, and statically unstable when the air is saturated, i.e.

$$\Gamma_{sat} < \Gamma < \Gamma_{dry}$$

where Γ_{sat} , Γ and Γ_{dry} represent the saturated, environmental and dry lapse rates ($-\partial T/\partial z$), respectively. Likewise, a combined temperature and velocity profile exhibits what we may define as conditional shearing instability (CSHI) at a particular height if the air is dynamically stable at that height when the air is unsaturated, and dynamically unstable when the air is saturated, i.e.

$$Ri_{sat} < Ri_{crit} < Ri_{dry}$$

where Ri_{dry} and Ri_{sat} represent the gradient Richardson Number calculated assuming the air is dry and saturated using values of static stability calculated from Eqs. 1 and 2, respectively. Ri_{crit} represents the critical Richardson Number, which will in general be a little less than $\frac{1}{4}$.

Similarly there is an analogy between potential instability (PI) and what we define as potential shearing instability (PSHI). PI exists over a layer in the atmosphere when the layer would be statically unstable if it were lifted to saturation. This might occur if the lower part of the layer became saturated before the upper part. The condition for PI to exist is $\partial\theta_w/\partial z < 0$. PSHI exists over a layer if the layer would become dynamically unstable, but not statically unstable, when it is lifted to saturation (assuming the shear over the layer remains constant). The layer does not need to exhibit CSHI at its original height for this to occur (although it may do) as the lower part of the layer may become saturated before the upper part due to a vertical gradient in relative humidity. This could dynamically destabilize the layer, without making it statically unstable.

In the case described, flow into the region containing billows was along the contours of the front-parallel component of wind (Fig. 4), indicating that the shear over the layer which became responsible for the billows was conserved as the layer was lifted to saturation. This layer, therefore, exhibited PSHI upstream of the billows, as well as CSHI. The concept of PSHI allows us to see that a dynamically stable layer can exhibit a latent dynamical instability. Only through lifting to saturation can this instability be released. This could, for example, also occur in a layer forced to ascend over or downwind of orography, making billows visible on the edges of orographic clouds (e.g. Reiter *et al.* 1969).

(d) *The generality of these results*

The warm front described, although a strong one associated with an ex-tropical cyclone, is not extraordinary, either in terms of the wind shear across it, or of the thermodynamic structure. It therefore seems likely that PSHI would exist and be released in many other warm fronts where ascent at the surface front induces saturation. Although billows are difficult to observe, there are a small number of published observations which appear to support this hypothesis. For example, Browning *et al.* (1970)

made Doppler radar observations in two precipitating warm frontal zones. Fairly large amplitude billows (with wavelengths up to 5 km) were observed ahead of the surface warm front, and can be seen in a cross-section parallel to the surface front in Fig. 7 of their paper. The billows observed by Bryant and Browning (1975) using Doppler radar occurred in a precipitating warm frontal zone, just ahead of the surface front. The layer containing billows had been brought to saturation at the time when they were observed. They were orientated perpendicularly to the surface front, and again, were caused by the component of shear parallel to the front. Takahashi *et al.* (1993) observed large-amplitude billows within a precipitating shear layer orientated parallel to a stationary surface front. Wang *et al.* (1983) observed long wavelength (12–19 km) billows within a precipitating warm frontal zone. They noted that the Richardson number calculated over the layer containing billows was sub-critical only if the effect of moisture was included.

In addition to these previously published observations and the main case study presented in this paper, Figs. 1(d) and (e) of this paper show RHIs of Doppler velocity and vertical shear obtained in another warm frontal case on 11 February 1997. The billows apparent in these RHIs again occurred in a precipitating warm frontal zone just ahead of the surface warm front. The mesoscale model's representation of this front (not shown) revealed that the air entering the region containing billows had been lifted to saturation by ascent at the warm front, although in this case the level of saturation was very close to the ground.

Studies of turbulent dissipation of kinetic energy in the free atmosphere have tended to concentrate on the dissipation by CAT, which is most likely to occur at frontal zones and near the tropopause close to jets. The stronger winds at upper levels rather than at lower levels might at first appear to suggest that the energy dissipation in the free atmosphere would be dominated by the contribution from higher levels. However, strong shears also occur in low-level frontal zones and the onset of saturation near surface fronts allows PSHI to be released over large depths, so significant mixing may occur. The frequency of occurrence of billows associated with surface fronts, and a quantitative estimate of the mixing that they induce should be the subject of further research.

ACKNOWLEDGEMENTS

We are grateful to Drs Anthony Illingworth and Mark Blackman for their part in the data acquisition, and thank the Radio Communications Research Unit at Rutherford Appleton Laboratory for access to the Chilbolton radar. We are also grateful to Peter Panagi for supplying the mesoscale model data. Daniel Chapman is supported by a studentship from the Natural Environment Research Council.

REFERENCES

- | | | |
|--|------|--|
| Atlas, D., Metcalf, J. I.,
Richter, J. H. and
Gossard, E. E. | 1970 | The birth of CAT and microscale turbulence. <i>J. Atmos. Sci.</i> , 27 , 903–913 |
| Blumen, W. | 1984 | An observational study of instability and turbulence in nighttime drainage winds. <i>Boundary-Layer Meteorol.</i> , 28 , 245–269 |
| Bosart, L. F. and Garcia, O. | 1974 | Gradient Richardson profiles and changes within an intense mid-tropospheric baroclinic zone. <i>Q. J. R. Meteorol. Soc.</i> , 100 , 593–607 |
| Browning, K. A. | 1971 | Structure of the atmosphere in the vicinity of large-amplitude Kelvin–Helmholtz billows. <i>Q. J. R. Meteorol. Soc.</i> , 97 , 283–299 |
| Browning, K. A. and Watkins, C. D. | 1970 | Observations of clear-air turbulence by high power radar. <i>Nature</i> , 227 , 260–263 |

- Browning, K. A., Harrold, T. W. and Starr, J. R. 1970 Richardson number limited shear zones in the free atmosphere. *Q. J. R. Meteorol. Soc.*, **96**, 40–49
- Browning, K. A., Bryant, G. W., Starr, J. R. and Axford, D. N. 1973a Air motion within Kelvin–Helmholtz billows determined from simultaneous Doppler radar and air-craft measurements. *Q. J. R. Meteorol. Soc.*, **99**, 619–638
- Browning, K. A., Hardman, M. E., Harrold, T. W. and Pardoe, C. W. 1973b The structure of rainbands within a mid-latitude depression. *Q. J. R. Meteorol. Soc.*, **99**, 215–231
- Bryant, G. W. and Browning, K. A. 1975 Multi-level measurements of turbulence over the sea during the passage of a frontal zone. *Q. J. R. Meteorol. Soc.*, **101**, 35–54
- Busak, B. and Brümmer, B. 1987 A case study of Kelvin–Helmholtz waves within an off-shore stable boundary layer: Observations and linear model. *Boundary-Layer Meteorol.*, **44**, 105–135
- Chapman, D. 1998 'Radar observations of mixing within frontal zones'. PhD Thesis, University of Reading
- Chapman, D. and Browning, K. A. 1997 Radar observations of wind-shear splitting within evolving atmospheric Kelvin–Helmholtz billows. *Q. J. R. Meteorol. Soc.*, **123**, 1433–1439
- Cullen, M. J. P. 1993 The unified forecast/climate model. *Meteorol. Mag.*, **122**, 81–94
- Davis, P. A. and Peltier, W. R. 1976 Resonant parallel shear instability in the stably stratified planetary boundary layer. *J. Atmos. Sci.*, **33**, 1287–1300
- Drazin, P. and Reid, W. 1981 *Hydrodynamic stability*. Cambridge University Press, London, UK
- Durrant, D. and Klemp, J. 1982 On the effects of moisture on the Brunt–Väisälä frequency. *J. Atmos. Sci.*, **39**, 2152–2158
- Fritts, D. C., Palmer, T. L., Andreassen, Ø. and Lie, I. 1996a Evolution and breakdown of Kelvin–Helmholtz billows in stratified compressible flows. I: Comparison of two- and three-dimensional flows. *J. Atmos. Sci.*, **53**, 3173–3191
- Fritts, D. C., Garten, J. F. and Andreassen, Ø. 1996b Wave breaking and transition to turbulence in stratified shear flows. *J. Atmos. Sci.*, **53**, 1057–1085
- Goddard, J. W. F., Eastment, J. D. and Thurai, M. 1994 The Chilbolton advanced meteorological radar: A tool for multi-disciplinary research. *Electron. Commun. Eng. J.*, **6**, 77–86
- Gossard 1990 Radar research on the Atmospheric Boundary Layer. Pp. 477–527 in *Radar in Meteorology*. Ed. D. Atlas. American Meteorological Society, Boston, USA
- Hardy, K. R., Reed, R. J. and Mather, G. K. 1973 Observation of Kelvin–Helmholtz billows and their mesoscale environment by radar, instrumented aircraft and a dense radiosonde network. *Q. J. R. Meteorol. Soc.*, **99**, 279–293
- James, P. K. and Browning, K. A. 1981 An observational study of primary and secondary billows in the free atmosphere. *Q. J. R. Meteorol. Soc.*, **107**, 351–365
- Keller, J. L. 1990 Clear air turbulence as a response to meso- and synoptic-scale dynamic processes. *Mon. Weather Rev.*, **118**, 2228–2242
- Kennedy, P. J. and Shapiro, M. A. 1980 Further encounters with clear air turbulence in research aircraft. *J. Atmos. Sci.*, **37**, 986–993
- Knox, J. A. 1997 Possible mechanisms of clear-air turbulence in strongly anticyclonic flows. *Mon. Weather Rev.*, **125**, 1251–1259
- Lalas, D. P. and Einaudi, F. 1974 On the correct use of the wet adiabatic lapse rate in stability criteria of a saturated atmosphere. *J. Appl. Meteorol.*, **13**, 318–324
- 1976 On the characteristics of gravity waves generated by atmospheric shear layers. *J. Atmos. Sci.*, **33**, 1248–1259
- Ludlam, F. H. 1967 Characteristics of billow clouds and their relation to clear air turbulence. *Q. J. R. Meteorol. Soc.*, **93**, 419–435
- 1980 *Clouds and Storms*. Pennsylvania State University Press, USA
- Metcalf, J. I. and Atlas, D. 1973 Microscale ordered motions and atmospheric structure associated with thin echo layers in stably stratified zones. *Boundary-Layer Meteorol.*, **4**, 7–35
- Miles, J. W. and Howard, L. N. 1964 Note on a heterogeneous shear flow. *J. Fluid Mech.*, **20**, 331–336
- Nielsen, J. W. 1992 In situ observations of Kelvin–Helmholtz waves along a frontal inversion. *J. Atmos. Sci.*, **49**, 369–386
- Readings, C. J. 1973 The formation and breakdown of Kelvin–Helmholtz billows (Working Group Report). *Boundary-Layer Meteorol.*, **5**, 233–240
- Reiter, E. R., Lester, P. F. and Wooldridge, G. 1969 Spectral analysis of a breaking wave. Pp. 21–33 in *Clear Air Turbulence and its Detection* Eds. Y.-H. Pao and A. Goldberg. Plenum Press, New York, USA

- Roach, W. T. 1970 On the influence of synoptic development on the production of high level turbulence. *Q. J. R. Meteorol. Soc.*, **96**, 413–429
- Scinocca, G. P. 1995 The mixing of mass and momentum by Kelvin–Helmholtz billows. *J. Atmos. Sci.*, **52**, 2509–2530
- Stull, R. B. 1988 *An introduction to boundary layer meteorology*. Kluwer Academic Publishers, Dordrecht, The Netherlands
- Sykes, R. I. and Lewellen, W. S. 1982 A numerical study of breaking Kelvin–Helmholtz billows using a Reynolds-stress turbulence closure model. *J. Atmos. Sci.*, **39**, 1506–1520
- Takahashi, N., Uyeda, H. and Kikuchi, K. 1993 A Doppler radar observation on wave-like echoes generated in a strong vertical shear. *J. Meteorol. Soc. Japan*, **71**, 357–365
- Thorpe, S. A. 1973 Turbulence in stably stratified fluids: A review of laboratory experiments. *Boundary-Layer Meteorol.*, **5**, 95–119
- 1987 Transitional phenomena and the development of turbulence in stratified fluids: A review. *J. Geophys. Res.*, **92**, 5231–5248
- Trout, D. and Panofsky, H. A. 1969 Energy dissipation near the tropopause. *Tellus*, **21**, 355–358
- Wang, P.-Y., Parsons, D. B. and Hobbs, P. V. 1983 The mesoscale and microscale structure and organization of clouds and precipitation in midlatitude cyclones. VI: Wave-like rainbands associated with a cold-frontal zone. *J. Atmos. Sci.*, **40**, 543–558